Sensitivity of the atmospheric response to warm pool El Niño events to modeled SSTs and future climate forcings

Margaret M. Hurwitz,[1,2] Chaim I. Garfinkel,[3,4] Paul A. Newman,[2] and Luke D. Oman[2]

[1] Warm pool El Niño (WPEN) events are characterized by positive sea surface temperature (SST) anomalies in the central equatorial Pacific. Under present-day climate conditions, WPEN events generate poleward propagating wavetrains and enhance midlatitude planetary wave activity, weakening the stratospheric polar vortices. The late 21st century extratropical atmospheric response to WPEN events is investigated using the Goddard Earth Observing System Chemistry-Climate Model (GEOSCCM), version 2. GEOSCCM simulations are forced by projected late 21st century concentrations of greenhouse gases (GHGs) and ozone-depleting substances (ODSs) and by SSTs and sea ice concentrations from an existing ocean-atmosphere simulation. Despite known ocean-atmosphere model biases, the prescribed SST fields represent a best estimate of the structure of late 21st century WPEN events. The future Arctic vortex response is qualitatively similar to that observed in recent decades but is weaker in late winter. This response reflects the weaker SST forcing in the Niño 3.4 region and subsequently weaker Northern Hemisphere tropospheric teleconnections. The Antarctic stratosphere does not respond to WPEN events in a future climate, reflecting a change in tropospheric teleconnections: The meridional wavetrain weakens while a more zonal wavetrain originates near Australia. Sensitivity simulations show that a strong poleward wavetrain response to WPEN requires a strengthening and southeastward extension of the South Pacific Convergence Zone; this feature is not captured by the late 21st century modeled SSTs. Expected future increases in GHGs and decreases in ODSs do not affect the polar stratospheric responses to WPEN.

Citation: Hurwitz, M. M., C. I. Garfinkel, P. A. Newman, and L. D. Oman (2013), Sensitivity of the atmospheric response to warm pool El Niño events to modeled SSTs and future climate forcings, *J. Geophys. Res. Atmos.*, *118*, 13,371–13,382, doi:10.1002/2013JD021051.

1. Introduction

[2] Warm pool El Niño (WPEN) events are characterized by positive sea surface temperature (SST) anomalies in the central equatorial Pacific and have occurred with increasing frequency in the past few decades [*Larkin and Harrison*, 2005; *Ashok et al.*, 2007; *Kug et al.*, 2009]. WPEN events are distinct from conventional or cold tongue El Niño events, typically with stronger, positive SST anomalies in the eastern equatorial Pacific [*Rasmusson and Carpenter*, 1982]. WPEN events modulate the extratropical climate [e.g., *Ashok et al.*, 2007; *Garfinkel et al.*, 2012].

[3] In the Southern Hemisphere (SH), WPEN events enhance convective activity in the South Pacific Convergence Zone in austral spring, forcing a tropospheric planetary wave that propagates toward SH high latitudes and upward into the Antarctic stratosphere [*Hurwitz et al.*, 2011a, 2011b]. This wave enhancement affects Antarctic surface temperatures [*Schneider et al.*, 2012] and sea ice concentrations [*Song et al.*, 2011] and leads to higher polar stratospheric temperatures and to a weaker polar jet during austral summer, as compared with neutral El Niño–Southern Oscillation (ENSO) years [*Hurwitz et al.*, 2011a, 2011b]. Enhanced planetary wave driving, higher polar lower stratospheric temperatures, and a weaker Antarctic jet have also been identified in response to a different definition of WPEN events. Specifically, *Zubiaurre and Calvo* [2012] and *Xie et al.* [2012] used the El Niño Modoki index [*Ashok et al.*, 2007], a different metric by which to identify WPEN events, and found SH responses consistent with *Hurwitz et al.* [2011a, 2011b].

[4] A recent model study by *Garfinkel et al.* [2012] determined that qualitatively, WPEN events have the same Northern Hemisphere (NH) impacts as conventional El Niño events: A deepened North Pacific tropospheric low and enhanced planetary wave driving in boreal winter, leading to a weakening of the Arctic vortex. Apparent contradictions in the findings of *Hegyi and Deng* [2011], *Xie et al.* [2012], and *Graf and Zanchettin* [2012] reflect both limitations in ENSO analysis when using the short observational

---

[1]Goddard Earth Sciences Technology and Research, Morgan State University, Baltimore, Maryland, USA.
[2]NASA Goddard Space Flight Center, Greenbelt, Maryland, USA.
[3]Johns Hopkins University, Baltimore, Maryland, USA.
[4]Now at Hebrew University, Jerusalem, Israel.

Corresponding author: M. M. Hurwitz, Goddard Earth Sciences Technology and Research, Morgan State University, Baltimore, MD 20771, USA. (margaret.m.hurwitz@nasa.gov)

Table 1. Summary of GEOSCCM Simulation Names and Boundary Conditions[a]

Simulation Name	GHGs	ODSs	SSTs and Sea Ice Composites
P_N	2005	2005	Hadley Centre Global Sea Ice and Sea Surface Temperature version 1 (HadISST1) (NTRL)
P_W	2005	2005	HadISST1 (WPEN)
$IDEAL_W$	2005	2005	HadISST1 (WPEN in the deep tropical Pacific; NTRL elsewhere)
F_N	2100	2100	Community Climate System Model version 3.0 (CCSM3) 2070–2100 (NTRL)
F_W	2100	2100	CCSM3 2070–2100 (WPEN)
$FSST_N$	2005	2005	CCSM3 2070–2100 (NTRL)
$FSST_W$	2005	2005	CCSM3 2070–2100 (WPEN)
$FCLI_N$	2100	2100	HadISST1 (NTRL)
$FCLI_W$	2100	2100	HadISST1 (WPEN)
A_N	2005	2100	HadISST1 (NTRL)
A_W	2005	2100	HadISST1 (WPEN)
B_N	2100	2100	Hadley Centre Global Environmental Model, version 1 (HadGEM1) 2070–2100 (NTRL)
B_W	2100	2100	HadGEM1 2070–2100 (WPEN)
C_N	2005	2005	CCSM3 2000–2030 (NTRL)
C_W	2005	2005	CCSM3 2000–2030 (WPEN)

[a]All are 50 year time slice simulations, as described in the text.

record and the sensitivity of the NH response to the precise definition of central Pacific El Niño events [*Garfinkel et al.*, 2012].

[5] Dramatic polar stratospheric climate change is expected by the end of the 21st century. Following moderate emissions scenarios, the atmospheric CO_2 concentration will approximately double while concentrations of ozone-depleting substances (ODSs) will be greatly reduced. While greenhouse gas (GHG)-related climate change will moderately cool the polar lower stratosphere in autumn, decreasing levels of ODSs will lead to ozone recovery and thus to warming trends in spring [*Hitchcock et al.*, 2009; *Hurwitz and Newman*, 2010]. Late 21st century changes in El Niño amplitude and frequency are unclear: The Coupled Model Intercomparison Project (CMIP5) models suggest no future trend in the overall ENSO amplitude [*Stevenson*, 2012], while other model studies predict that the pattern of 21st century SST trends will favor central Pacific warming [*Yeh et al.*, 2009; *Xie et al.*, 2010]. If so, in the polar stratosphere, the dynamical warming associated with frequent WPEN events would offset some of the predicted radiative cooling by GHGs.

[6] Not only may the frequency of WPEN events change in a future climate but also may the tropospheric planetary wave response. Several model studies predict that the NH circulation response (i.e., teleconnections) to strong ENSO events will change under enhanced CO_2 conditions [e.g., *Collins*, 2000; *Müller and Roeckner*, 2006; *Kug et al.*, 2010].

[7] Since WPEN events have contributed to polar stratospheric variability in recent decades, a thorough evaluation of the extratropical impacts of these events in a late 21st century climate will improve overall estimates of future variability. This paper describes the future polar stratospheric response to WPEN events, as simulated by the Goddard Earth Observing System Chemistry-Climate Model (GEOSCCM), and uses idealized and sensitivity simulations to pinpoint the causes of potential changes in the WPEN response due to modeled SST fields and future climate conditions. The model and simulations are described in section 2. Section 3 presents the results, comparing WPEN and ENSO neutral simulations, under present, future, and idealized climate conditions. Section 4 presents a brief summary and discussion.

2. Model Description and GEOSCCM Simulations

2.1. Model Description

[8] The Goddard Earth Observing System Chemistry-Climate Model, (GEOSCCM) version 2 couples the GEOS-5 atmospheric general circulation model (GCM) [*Rienecker et al.*, 2008; *Molod et al.*, 2012] and a comprehensive stratospheric chemistry scheme [*Kawa et al.*, 2003; *Pawson et al.*, 2008]. The model is run at 2° latitude × 2.5° longitude horizontal resolution and 72 vertical layers, with a model top at 0.01 hPa. Predicted distributions of water vapor, ozone, the primary greenhouse gases (CO_2, CH_4, and N_2O), CFC-11, CFC-12, and HCFC-22 feed back to the radiative calculations. The GEOSCCM performed well in the *Stratospheric Processes and their Role in Climate (SPARC) Chemistry-Climate Model Validation (CCMVal)* [2010] detailed evaluation of stratospheric processes.

[9] The present study uses the formulation of the GEOSCCM as documented by *Hurwitz et al.* [2011b]. Specifically, the stratospheric chemistry module is the same as that documented by *SPARC CCMVal* [2010], while the GEOS-5 GCM has been updated. The updated GCM generates a spontaneous quasi-biennial oscillation, with a realistic period (27 months at 30 hPa and 50 hPa [*Hurwitz et al.*, 2013]) and zonal wind amplitude, and improved tropospheric stationary wave patterns in the Southern Hemisphere. This formulation of the GEOSCCM has been successfully used to evaluate the response of the Antarctic stratosphere to warm pool El Niño events in a present-day climate [*Hurwitz et al.*, 2011b], compare the NH responses to central Pacific and eastern Pacific El Niño events [*Garfinkel et al.*, 2012], and isolate the impact of North Pacific SSTs on the Arctic winter climate [*Hurwitz et al.*, 2012].

2.2. GEOSCCM Simulations

[10] Nine GEOSCCM simulations, plus six supplementary simulations, are used to isolate the impact of WPEN events on the upper troposphere and polar stratosphere, in present-day and likely future climate conditions (Table 1). All simulations are 50-year time slices, with fixed concentrations of the primary greenhouse gases (GHGs) and ozone-depleting substances (ODSs), and sea surface temperature (SST) and sea ice fields with repeating annual cycles. This experimental
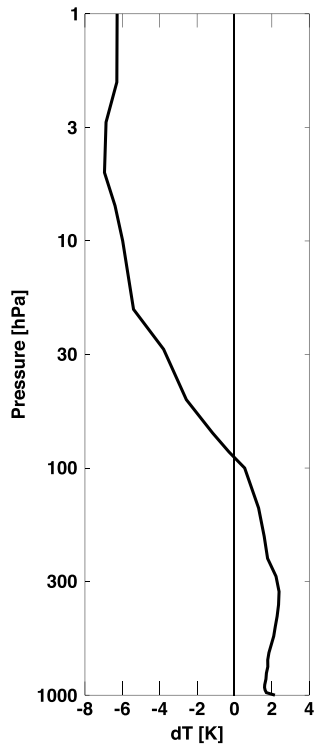
Figure 1. F_N-P_N global and annual mean temperature differences (K).

design provides large samples of the atmospheric response to each set of climate conditions. Pairs of simulations each contain a WPEN simulation and an ENSO neutral (NTRL) simulation, with SST and sea ice fields generated by compositing WPEN or NTRL events, respectively. Each ENSO event included in the climatologies spans from the July preceding the boreal winter peak in tropical SST anomalies through June of the following year.

[11] A first pair of simulations represents the present-day climate ("P"). As reported by *Hurwitz et al.* [2011b], 2005 GHG and ODS concentrations are prescribed in both simulations, but the prescribed SST and sea ice conditions are distinct. The 1991–1992 and 1994–1995 WPEN events are composited to create the SST and sea ice climatologies used as boundary conditions for the P_W simulation; SST and sea ice concentrations are derived from HadISST1 [*Rayner et al.*, 2003]. Similarly, 10 NTRL events spanning the 1979–2011 period are composited to create SST and sea ice climatologies used as boundary conditions in the P_N simulation.

[12] An additional, idealized WPEN simulation ("IDEAL$_W$"; "CPWideal" in *Garfinkel et al.* [2012]) is compared with P_N. Differences between IDEAL$_W$ and P_N isolate the contribution of deep tropical central Pacific SST anomalies to the atmospheric WPEN teleconnections. In IDEAL$_W$, SSTs between 10°N, 10°S, 140°E, and 240°E are identical to those in the P_W simulation. SSTs poleward of 20° latitude, west of 115°E and east of 265°E are identical to those in the P_N simulation. Between these two regions, SSTs in IDEAL$_W$ are linearly interpolated between the P_W and P_N climatologies.

[13] A second pair of simulations represents the expected late 21st century or "future" climate ("F"). Concentrations of GHGs [A1B scenario; *Solomon et al.*, 2007] and ODSs [A1 scenario; *World Meteorological Organization*, 2011]

are both fixed at 2100 values. SSTs and sea ice are taken from the Community Climate System Model, version 3.0 (CCSM3) (http://www.ccsm.ucar.edu), of the Coupled Model Intercomparison Project, phase 3 (CMIP3) (http://www-pcmdi.llnl.gov/ipcc/about_ipcc.php) A1B scenario simulations of the 21st century, for the 2070–2100 period. WPEN and NTRL events are identified using similar criteria as for observed events: WPEN events are identified when the September-October-November (SON) seasonal mean Niño 4 index (monthly SST anomalies in the 5°S–5°N, 160°–210°E region; http://www.cpc.ncep.noaa.gov/data/indices/) exceeds one standard deviation from the 2070–2100 mean and is larger than the equivalent Niño 3 index (monthly SST anomalies in the 5°S–5°N, 210°–270°E region). NTRL events are identified when the SON seasonal mean Niño 3 and Niño 4 indices are both within 0.7 standard deviations from the respective 2070–2100 means. The 6 WPEN and 12 NTRL events are composited to create SST and sea ice boundary conditions, respectively, for the F_W and F_N simulations.

[14] The future simulations represent large changes in the global and annual mean temperature from the present day. Specifically, Figure 1 shows differences between the NTRL future simulation and the NTRL present simulation (i.e., F_N–P_N). The troposphere warms by approximately 2 K, while strong stratospheric cooling increases with height, exceeding 7 K in the upper stratosphere.

[15] Differences in tropical Pacific SSTs, as prescribed in the WPEN and NTRL simulations, are shown in Figure 2. By definition, WPEN–NTRL SST differences are positive in the central equatorial Pacific (i.e., Niño 4 region), in the present-day (Figures 2a and 2d), idealized present-day (Figures 2b and 2e), and future (Figures 2c and 2f) cases, with SST differences exceeding 1 K in some regions in boreal winter. SON (December-January-February (DJF)) seasonal mean Niño 4 anomalies are comparable in the three sets of SST anomalies: 0.76 K (0.89 K) in the P simulations, 0.73 K (0.83 K) in IDEAL$_W$, and 0.76 K (0.83 K) in the F simulations (Table 4). Outside of the deep tropical Pacific, SST anomalies differ between the various simulations.

[16] Two additional pairs of simulations separate the impacts of changing radiative forcing and modeled late 21st century SSTs on the polar stratospheric response to WPEN (Table 1). In the "FCLI" simulations, present-day SSTs are prescribed (Figures 2a and 2d), with 2100 values for the GHGs and ODSs. In the "FSST" simulations, modeled late 21st century SSTs are prescribed (Figures 2c and 2f), with 2005 values for the GHGs and ODSs.

[17] Six supplementary simulations test the sensitivity of the WPEN teleconnections to ozone recovery (section 3.3) and to the choice of prescribed SST fields (section 3.4). The "A" pair of simulations (Table 1) tests the sensitivity to ozone recovery. These simulations are forced with observed SSTs and 2005 values of GHGs, but with projected 2100 values of ODSs. The "B" pair of simulations (Table 1) is identical to the F simulations, except that the late 21st century SSTs are taken from a Hadley Centre Global Environmental Model, version 1 (HadGEM1) simulation, as is further discussed in section 3.4. The "C" pair of simulations is identical to the P simulations, except that early 21st century modeled SSTs from CCSM3 are used in place of observed SSTs.
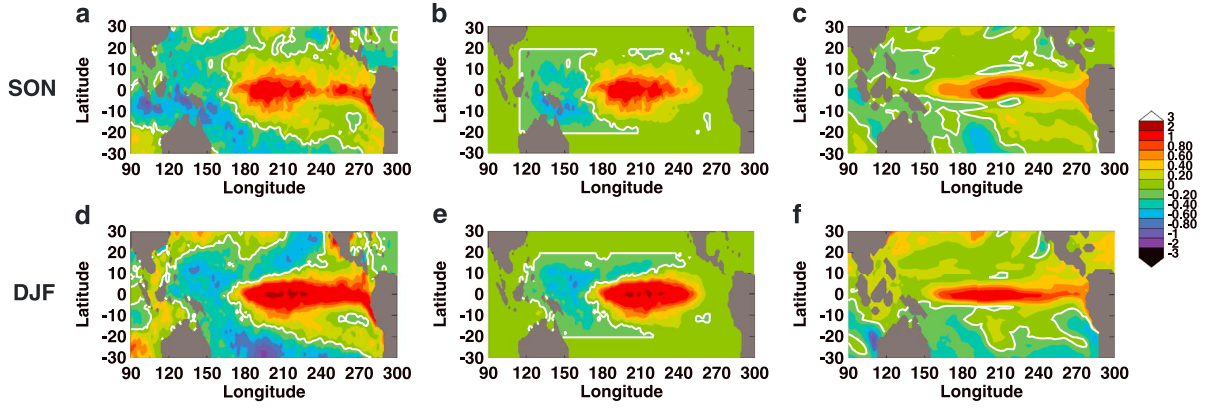
Figure 2. WPEN-NTRL SST differences in the (a–c) SON season and (d–f) DJF season. SST differences prescribed in the (a and d) P and FCLI simulations, (b and e) IDEALw - Pw, and (c and f) F and FSST simulations.

3. Results

3.1. Polar Stratospheric Response to WPEN

[18] In the present-day simulations, the polar vortex weakens in response to WPEN events, i.e., positive WPEN-NTRL geopotential height differences poleward of 60° latitude in both the Arctic (Figure 3a) and Antarctic (Figure 3b). The Arctic response to WPEN events is strongest in late boreal winter [*Garfinkel et al.*, 2012], while in the Antarctic the response to WPEN events is strongest in austral spring [*Hurwitz et al.*, 2011b]. In the upper stratosphere, the magnitude of the Arctic response is greater than the Antarctic response. In the Arctic, these geopotential height differences correspond with lower stratospheric polar cap temperature
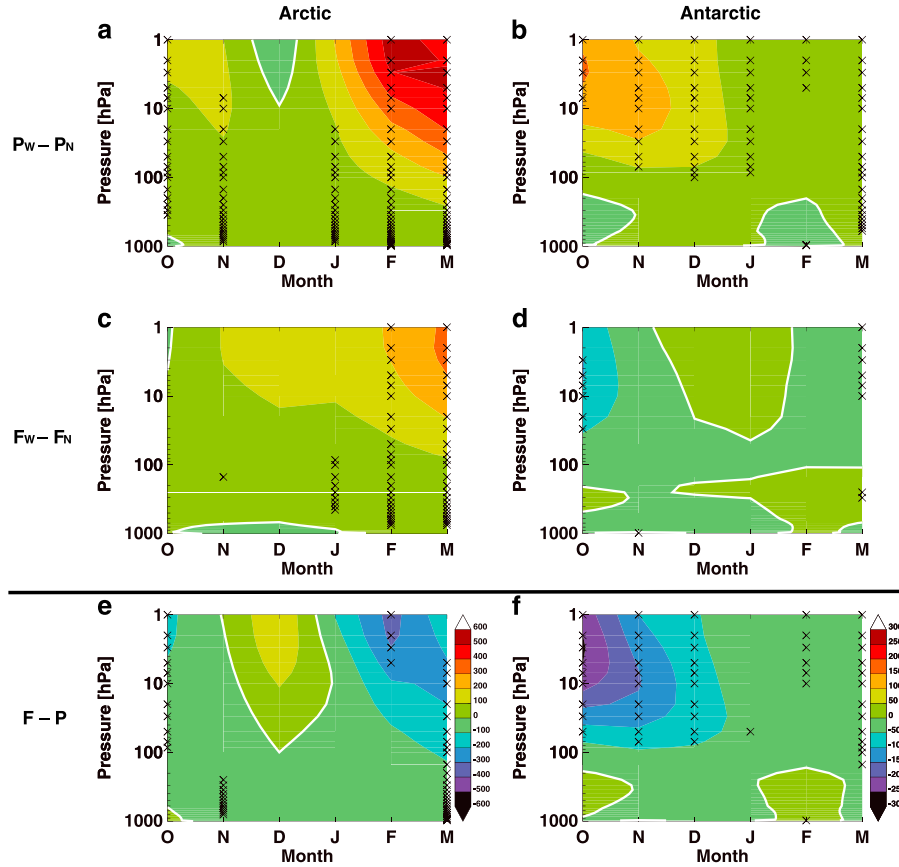

Figure 3. WPEN-NTRL polar cap geopotential height differences, in October through March, as a function of altitude (m). (a and b) P simulations, (c and d) F simulations, (e and f) F-P differences. Note the different color scales for the Arctic in Figures 3a, 3c, and 3e and Antarctic in Figures 3b, 3d, and 3f. White contours indicate zero difference. Black crosses indicate differences significant at the 95% level, in a two-tailed *t* test.
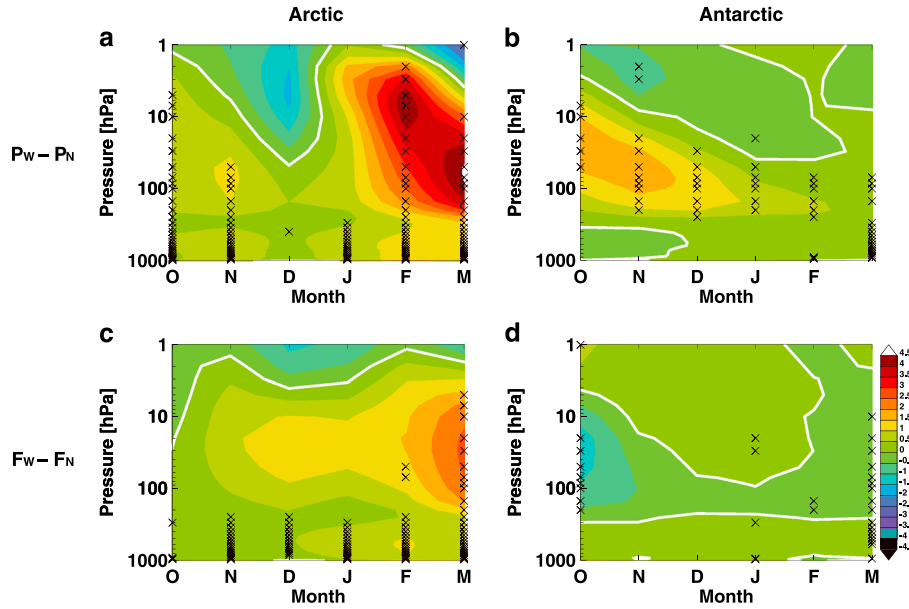
Figure 4. WPEN-NTRL polar cap temperature differences, in October through March, as a function of altitude (K). (a and b) P simulations. (c and d) F simulations. White contours indicate zero difference. Black crosses indicate differences significant at the 95% level, in a two-tailed *t* test.

increases of approximately 1 K in the early and midwinter, and a larger 3–4 K warming in February and March (Figure 4a). The Antarctic lower stratosphere warms by 1–2 K, with the largest temperature differences in October through December (Figure 4b).

[19] The polar stratospheric response to WPEN events changes in a future climate. Figures 3c, 3d, 4c, and 4d show the equivalent WPEN responses in the future simulations, while Figures 3e and 3f show differences between the future and present-day geopotential height responses. In the Arctic, future WPEN events continue to weaken and warm the polar vortex (Figures 3c and 4c), though the response is weaker than that simulated in a present-day climate in October, February, and March (Figure 3e). In the lower stratosphere, the polar cap temperature response to WPEN is approximately 1–2 K. In the F simulations, warming of the Antarctic lower stratospheric response is replaced by weak cooling in October and a null response in later months (Figures 3d and 4d). The remainder of section 3 will make use of the idealized and sensitivity simulations to explain the simulated future changes in the polar stratospheric responses to WPEN.

3.2. Tropospheric WPEN Teleconnections

[20] Future changes in the polar stratospheric response to WPEN events reflect changes in tropospheric planetary wave driving, which in turn reflect changes in the tropospheric circulation response pattern (or "teleconnections") to WPEN events. Because the Arctic stratospheric response to WPEN is strongest in late boreal winter, the Northern Hemisphere (NH) tropospheric responses are examined for the preceding months (i.e., the DJF season). Because the Antarctic stratospheric response is strongest in austral early summer, the Southern Hemisphere (SH) tropospheric responses are examined for the SON season.

[21] Under present-day conditions, WPEN events generate a strong poleward, upper tropospheric wavetrain response in the NH in boreal winter, i.e., increased geopotential heights in the tropical central Pacific, a low centered at 40°N, 220°E, and increased heights centered at 60°N, 250°E (Figure 5a; see also *Garfinkel et al.* [2012]). The first temporal empirical orthogonal function (EOF) of WPEN-NTRL differences in the P simulations highlights this poleward wavetrain pattern (Figure 5e). Planetary wave activity in the North Pacific is enhanced during observed WPEN events. Figure 6 shows the results of Rossby wave source calculations [based on *Jin and Hoskins*, 1995] derived from the simulated upper tropospheric wind fields. The average of the 250 hPa and 300 hPa pressure levels is shown [as in *Hurwitz et al.*, 2011b], as the 250 hPa and 300 hPa levels emphasize differences at mid-latitudes. Rossby wave source is a concise way of determining the forcing by Rossby waves, due to the divergent component of the flow. The deepened North Pacific low is located downstream of a Rossby wave source (Figure 6a). Another measure of tropospheric planetary wave driving is the December/January mean eddy heat flux at 40–80°N, 100 hPa [*Newman et al.*, 2001]: Eddy heat flux is enhanced in response to WPEN events (i.e., $P_W - P_N$), in a contemporary climate (Table 2).

[22] Under future climate conditions, the NH tropospheric response retains the same pattern but weakens, consistent with the polar stratospheric response. Specifically, in the F simulations, the upper tropospheric geopotential height response to WPEN strongly resembles the response in the P simulations (compare Figures 5a and 5d). The first EOF of the $F_W - F_N$ response (Figure 5f) is indistinguishable from the first EOF of $P_W - P_N$ (Figure 5e); the two patterns are correlated with $r = 0.92$. In the future simulations, WPEN enhances tropospheric wave driving (Table 2); however, the North Pacific Rossby wave source response to WPEN is weaker in the future simulations (Figure 6d), as are the geopotential height differences at 60°N, 250°E, than in the present-day simulations.
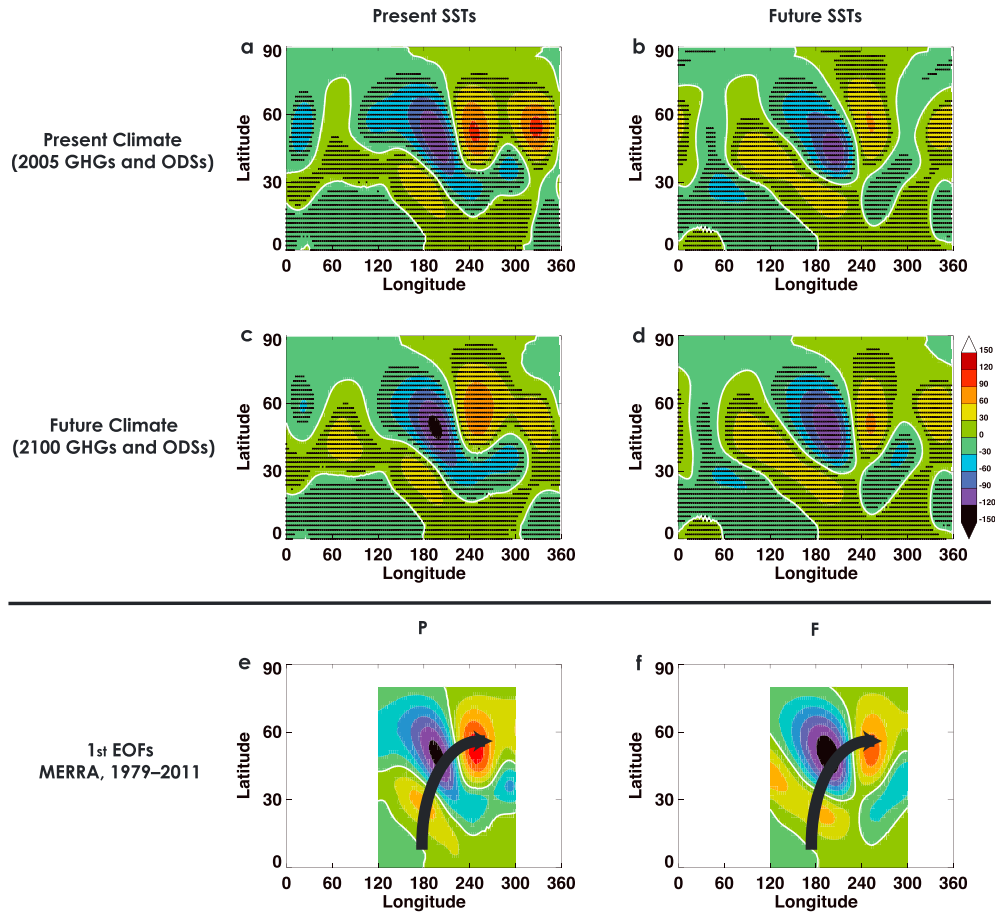
Present SSTs

Future SSTs

Figure 5. (a–d) WPEN-NTRL 250 hPa geopotential height differences (m) in the DJF season in the (a) P simulations, (b) FSST simulations, (c) FCLI simulations, and (d) F simulations. White contours indicate zero difference. Black crosses indicate differences significant at the 95% level, in a two-tailed t test. (e–f) Temporal first EOFs of WPEN-NTRL geopotential height differences in the North Pacific, at 250 hPa: P and F in Figures 5e and 5f, respectively; thick, black arrows indicate the approximate direction of the poleward wavetrains.
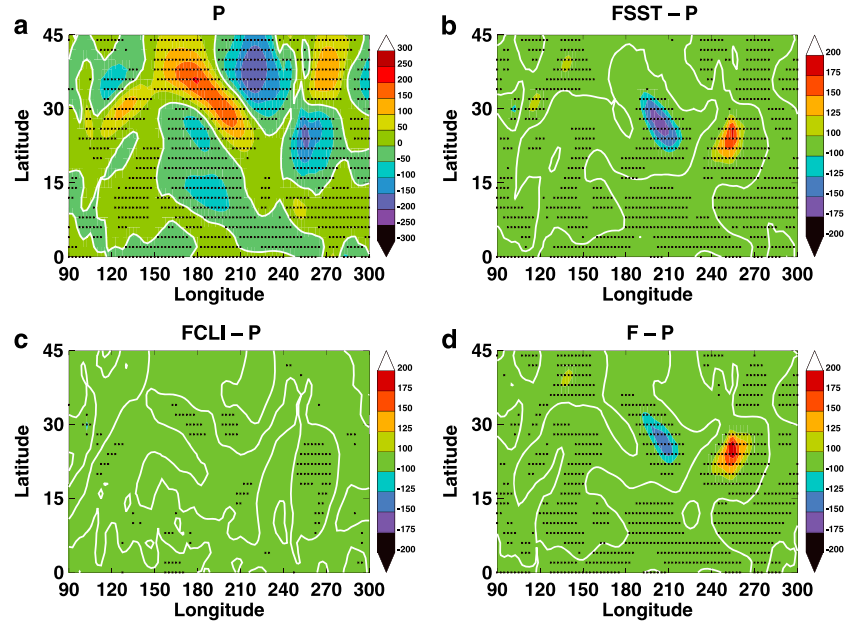
Figure 6. WPEN-NTRL differences in DJF upper tropospheric Rossby wave source [10^{10} s^{-2}], as described in the text, in (a) P simulations, (b) FSST-P differences, (c) FCLI-P differences, and (d) F-P differences. Black crosses indicate differences significant at the 95% level, in a two-tailed t test. White contours indicate zero difference.

Table 2. Magnitude of the December/January Eddy Heat Flux at 40–80°N, 100 hPa[a]

Pair of Simulations	WPEN	NTRL
P	11.01 ± 0.22	10.28 ± 0.25
F	14.01 ± 0.38	13.21 ± 0.35
FCLI	13.50 ± 0.40	11.88 ± 0.34
FSST	14.43 ± 0.37	13.42 ± 0.45

[a]WPEN-NTRL differences are statistically significant at the 95% level in the P, FCLI, and FSST simulations, and at the 85% level in the F simulations, based on two-tailed t tests.

[23] Sensitivity simulations suggest that it is the change in the prescribed SST field, rather than the change in ODS or GHG concentrations that modifies the stratospheric response to WPEN events. In the FCLI simulations, where present-day SST climatologies are prescribed under future GHG and ODS concentrations, Rossby wave source differences are indistinguishable from the present-day differences (Figure 6c). In the FSST simulations, where future SST climatologies are prescribed under present-day GHG and ODS concentrations, the North Pacific Rossby wave source weakens (Figure 6b and Table 2), as in the F simulations.

[24] Weaker upper tropospheric and Arctic stratospheric responses to WPEN, in the simulations where late 21st century modeled SSTs are prescribed, are caused by weaker tropical SST forcing and not by future SST changes and/or model biases outside of the tropical Pacific. Table 4 shows that while the prescribed SST differences in the Niño 4 region in various simulations are comparable for the DJF season (i.e., 0.89 K and 0.83 K), as chosen by the experimental design, SST differences directly to the east, i.e., in the Niño 3.4 region (5°S–5°N, 190°–240°E; http://www.cpc.ncep.noaa.gov/data/indices/) are nearly twice as large in the simulations forced by observed SSTs (i.e., 1.60 K) than in the

simulations forced by modeled late 21st century SSTs (0.90 K). That is, the magnitude of the extratropical atmospheric response to WPEN depends on the SST forcing in the Niño 3.4 region. Conversely, the WPEN response is not sensitive to extratropical SST differences: The present-day structure and magnitude of the upper tropospheric response and subsequent warming of the Arctic stratosphere (Figures 4a and 5a) are seen in the idealized WPEN simulation (Figure 7).

[25] As for the NH response, WPEN events generate a strong poleward, upper tropospheric wavetrain response in the South Pacific in austral spring. Geopotential height increases in the tropical, central South Pacific, decreases around 40°S, 210°E, and increases around 60°S, 240°E (Figure 8a; see also *Hurwitz et al.* [2011a, 2011b]). The first temporal empirical orthogonal function (EOF)) of WPEN-NTRL differences in the P simulations highlights this poleward wavetrain pattern (Figure 8e). This pattern resembles the Pacific-South America-1 (PSA-1) pattern, as identified by *Mo* [2000] and *Vera et al.* [2004], and is the second leading mode of observed interannual variability in the South Pacific region. As for the North Pacific low, the deepened South Pacific low at 40°S, 210°E is fed by an anomalous Rossby wave source (Figure 9a). The Rossby wave source results from the strengthening of convective activity in the southeastern South Pacific Convergence Zone (SPCZ), in response to WPEN events [*Hurwitz et al.*, 2011a]. Figure 10a shows the WPEN-related decrease in outgoing longwave radiation (OLR) (a proxy for increased convection) in the tropical central Pacific and in the diagonal region between 15°S, 220°E, and 40°S, 270°E, in the P simulations. Furthermore, at high latitudes, the structure of the geopotential height anomalies is in phase with the climatological field [*Zubiaurre and Calvo*, 2012] enhancing wave driving to the stratosphere: October/November eddy heat flux at 40–80°S, 100 hPa increases in response to WPEN (Table 3).
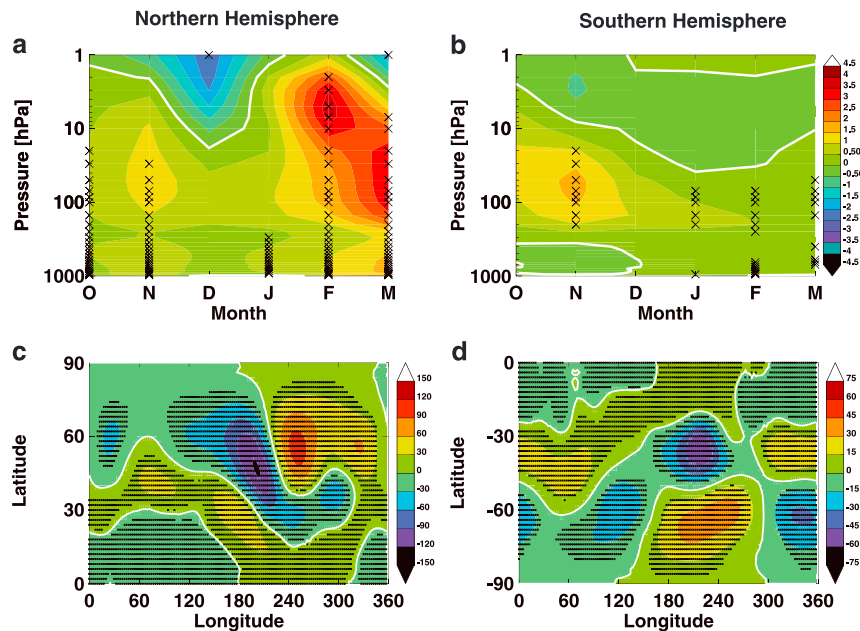

Figure 7. (a and b) IDEAL$_W$-P$_N$ differences in polar cap temperature, in October through March, as a function of altitude (K). (c) DJF geopotential height anomalies at 250 hPa and (d) SON geopotential height anomalies at 250 hPa. White contours indicate zero difference. Black crosses indicate differences significant at the 95% level, in a two-tailed t test.
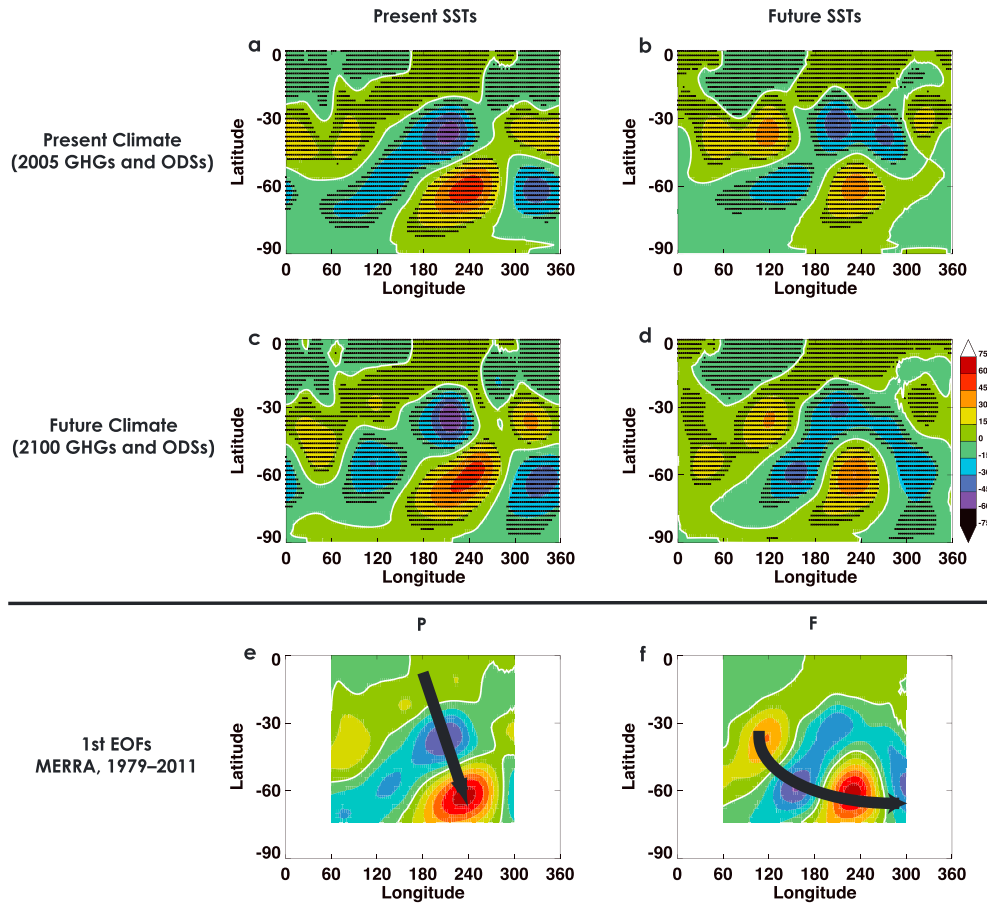
Figure 8. (a–d) WPEN-NTRL 250 hPa geopotential height differences (m) in the SON season in the (a) P simulations, (b) FSST simulations, (c) FCLI simulations, and (d) F simulations. White contours indicate zero difference. Black crosses indicate differences significant at the 95% level, in a two-tailed t test. (e–f) Temporal first EOFs of WPEN-NTRL geopotential height differences in the South Pacific, at 250 hPa: P, with dominant poleward wavetrain (PSA-1) in Figure 8e and F with dominant zonal wavetrain (PSA-2) in Figure 8f. Thick, black arrows indicate the approximate direction of the PSA-1-like and PSA-2-like wavetrains, respectively.

[26] When late 21st century SSTs and 2100 climate conditions are prescribed (Figure 8d), the structure of the poleward wavetrain response remains but with significantly smaller geopotential height differences at 40°S and 60°S. In addition, a region of positive height differences is seen around Australia (30°S, 120°E), part of a more zonal wavetrain with negative height differences around 60°S, 150°E, positive height differences around 60°S, 240°E, and negative differences around 70°S, 300°E. The dominant mode of variability of the $F_W - F_N$ differences i.e., the 1st temporal empirical orthogonal function (EOF)) highlights this zonal wavetrain pattern (Figure 8f). The 1st EOF pattern resembles the Pacific-South America-2 (PSA-2) mode of observed variability [*Mo*, 2000; *Vera et al.*, 2004]. Corresponding with the changes in the upper tropospheric teleconnection pattern, the Rossby wave source at 30°S, 240°E weakens in the F simulations relative to the P simulations, and a relative Rossby wave source appears around 30°S, 110°E (Figure 9d).

[27] As for the Northern Hemisphere teleconnections, sensitivity simulations suggest that it is the change in South Pacific SSTs rather than the change in ODS or GHG concentrations that modifies the tropospheric response and ultimately the stratospheric response to WPEN events in the SH. In the FCLI simulations, the WPEN teleconnection pattern resembles the present-day response (compare Figures 8a and 8c), with a strong poleward (i.e., PSA-1-like) geopotential height pattern. The pattern of the temporal first EOF of WPEN-NTRL differences in the FCLI simulations is strongly correlated with that in the P simulations ($r = 0.94$). As in the present-day simulations [*Hurwitz et al.*, 2011b], strong poleward planetary wave activity leads to a significant increase in eddy heat flux at 40–80°S, 100 hPa in October/November during WPEN events (Table 3). The South Pacific Rossby wave source at 30°S, 240°E in fact strengthens slightly (Figure 9).

[28] The tropospheric response to WPEN changes when late 21st century modeled SSTs are prescribed. In the FSST simulations, the WPEN teleconnection pattern most resembles the future climate response: a weaker PSA-1-like response as well as a strong, zonal PSA-2-like response (compare Figure 8). The pattern of the temporal first EOF in the FSST simulations is strongly correlated with that in the F simulations ($r = 0.91$). Weakening of the PSA-1-like response weakens the tropospheric planetary wave driving of the stratosphere, leading to insignificant eddy heat flux responses to WPEN events in the FSST and F simulations (Table 2).
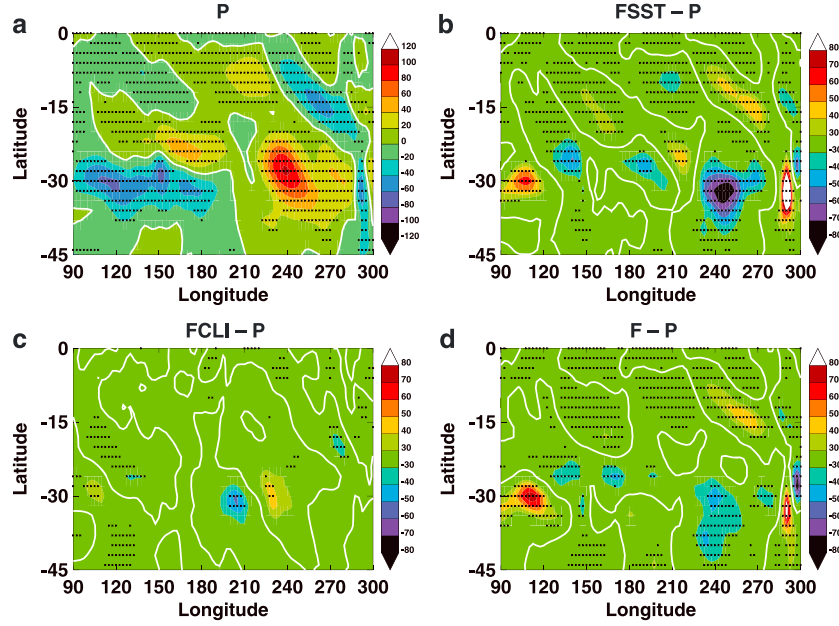
Figure 9. WPEN-NTRL differences in SON upper tropospheric Rossby wave source $[10^{10}\,\mathrm{s}^{-2}]$, as described in the text, in (a) P simulations, (b) FSST-P differences, (c) FCLI-P differences, and (d) F-P differences. Black crosses indicate differences significant at the 95% level, in a two-tailed t test. White contours indicate zero difference.

[29] A strong meridional wavetrain response requires positive SST forcing from the south-central Pacific, in the region 200–240°E, 10–20°S. The present-day and idealized simulations are forced by positive SST anomalies in the south-central Pacific (180–220°E, 5–20°S; see Figures 2a and 2b), while SST anomalies in the simulations forced by modeled late 21st century SSTs lack sufficiently positive SST anomalies in this region (Figure 2c). This difference in SST forcing leads to a weaker convective response in the southeastern South Pacific Convergence Zone (i.e., the region of 240°E, 30°S) than in the present-day simulations (compare Figures 10c and 10d with Figures 10a and 10b), and thus to a much weaker Rossby wave source (e.g., Figures 9b and 9d), weaker meridional

wavetrain response (Figures 8b and 8d) and ultimately to the failure to warm the Antarctic lower stratosphere (compare Figure 4d to Figures 4b and 7).

[30] The appearance of the zonal PSA-2-like wavetrain response in the simulations forced by late 21st century SSTs (see Figure 8), with positive geopotential height differences at 30°S, 120°E, suggests a heating anomaly near Australia. Figure 11 shows the 2 m (i.e., surface) temperature responses to WPEN events in the present-day, idealized and future simulations in austral spring. Note the striking Australian temperature anomaly exceeding 2 K in the F simulations, as compared with the present-day and idealized simulations. These Australian heating anomalies are seen throughout the
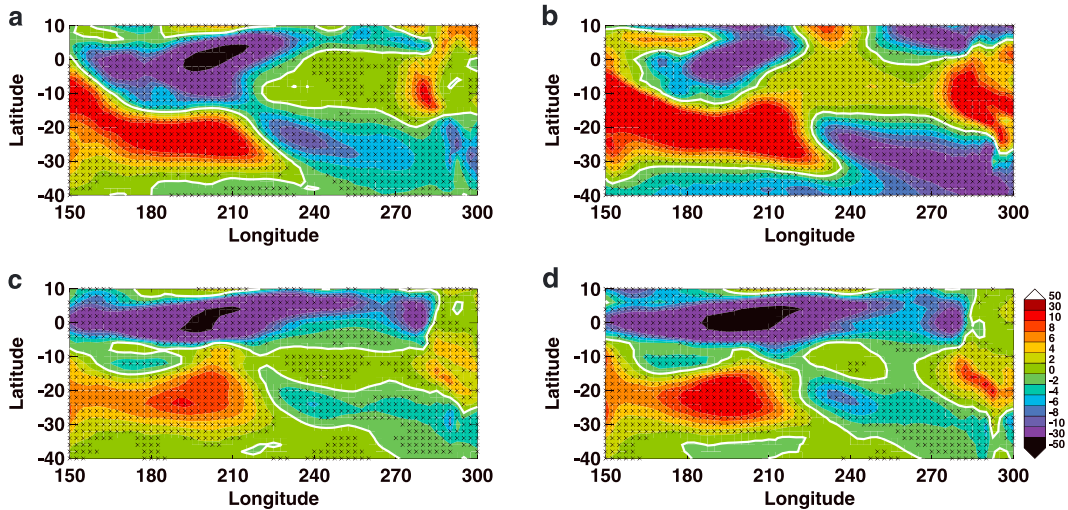

Figure 10. WPEN-NTRL differences in SON seasonal mean OLR $(\mathrm{W\,m^{-2}})$ for (a) P_W-P_N, (b) IDEAL$_W$-P_N, (c) FSST$_W$-FSST$_N$, and (d) F_W-F_N. Black crosses indicate differences significant at the 95% level, in a two-tailed t test. White contours denote zero difference.

Table 3. Magnitude of the October/November Eddy Heat Flux at 40–80°S, 100 hPa[a]

Pair of Simulations	WPEN	NTRL
P	7.32 ± 0.22	6.80 ± 0.26
F	7.08 ± 0.19	6.89 ± 0.24
FCLI	7.26 ± 0.22	6.39 ± 0.22
FSST	6.99 ± 0.20	6.86 ± 0.20

[a]WPEN-NTRL differences are statistically significant at the 85% (99%) level in the P (FCLI) simulations, based on two-tailed t tests.

tropospheric column, i.e., consistent with the appearance of a Rossby wave source at 30°S, 110°E (Figures 9b and 9d).

3.3. Sensitivity to Ozone Recovery

[31] The previous section showed that in the GEOSCCM, the extratropical atmospheric response to WPEN is insensitive to predicted future changes in GHG and ODS concentrations. The WPEN response might lack sensitivity to climate change because the impacts of simultaneously decreasing ODSs (ozone recovery, weakening of the polar vortices and equatorward shifting of the tropospheric midlatitude jet) and increasing GHGs (strengthening of the polar vortices and poleward shifting of the tropospheric jet) may cancel out each other [*Polvani et al.*, 2011; *Arblaster et al.*, 2011]. To test this hypothesis, an additional pair of GEOSCCM simulations ("A"; Table 1) was performed. This pair of simulations isolates the impact of ozone recovery on the polar stratospheric response to WPEN events, by prescribing present-day SSTs and GHGs but projected 2100 values for the ODSs.

[32] In isolation, ozone recovery has a negligible impact on the tropospheric and stratospheric responses to WPEN (not shown). While Antarctic ozone recovery (i.e., additional radiative heating by stratospheric ozone) warms the polar stratosphere, it has no impact on the Antarctic stratospheric response to WPEN: The response under ozone recovery is indistinguishable from the present-day simulations.

3.4. Sensitivity to the Prescribed SST Fields

[33] The results presented in sections 3.1 and 3.2 suggest that the atmospheric response to WPEN is sensitive to the prescribed SST field. However, only one pair of modeled SST fields was tested in the set of simulations as described above. Two additional pairs of simulations were performed for comparison with the F simulations. Together, these three pairs of simulations measure, to some degree, the sensitivity of the results to the prescribed set of modeled SSTs.

[34] The first pair of simulations ("B"; Table 1) is forced with 2100 values of GHGs and ODSs, and late 21st century SSTs. SSTs and sea ice are taken from a Hadley Centre Global Environmental Model, version 1 (HadGEM1) simulation [*Johns*, 2006] using the 2070–2100 period of a A1B scenario simulation. WPEN and NTRL events are identified as for the F simulations; 6 WPEN and 10 NTRL events are composited to create the SST and sea ice boundary conditions. WPEN−NTRL SST anomalies in the Niño 4 and Niño 3.4 regions are comparable to those in the F simulations (Table 4). Note that future simulations forced with HadGEM1 SSTs [*Johns*, 2006] yield nearly identical changes in global mean temperature, despite the higher climate sensitivity to doubled CO_2 in HadGEM1 than in CCSM3 [*Kiehl et al.*, 2006], due to cold biases in the present-day climate.

[35] The second pair of simulations ("C"; Table 1) is forced with 2005 values of GHGs and ODSs, and early 21st century SSTs. SSTs and sea ice values are taken from the CCSM3 A1B scenario simulation, as in the F simulations, but for the 2000–2030 period. The 4 WPEN and 10 NTRL events are composited to create the SST and sea ice boundary conditions.

[36] The B and C pairs of simulations, forced with HadGEM1 and CCSM3 SSTs, yield qualitatively similar atmospheric responses to WPEN as in the F simulations. The poleward, upper tropospheric wavetrains are weaker than in the P simulations, weakening planetary wave driving of the stratosphere. Compared with the P simulations, the Arctic vortex warms less in late boreal winter. This result is consistent with the weaker SST anomalies in the Niño 3.4 region during the DJF season (0.57 K and 0.61 K, in the two additional pairs of simulations, respectively) as compared with the observed anomalies (1.60 K) (Table 4). Figure 12a shows the positive relationship between SST anomalies in the Niño 3.4 region and the late winter Arctic stratospheric temperature response.

[37] The Antarctic stratosphere does not warm in the B and C simulations with modeled SSTs. In the C simulations, the magnitude of the SST anomalies in the south-central Pacific is weaker than observed, leading to a weak convective response in the SPCZ region and consequently to a weak planetary wave response at high latitudes (Figure 12b). In the B simulations, the magnitude of the south-central Pacific SST anomaly resembles that in the observations. However, in B_N, the high-latitude stationary wave patterns are not well simulated. Destructive interference between the patterns in B_N and B_W inhibits the propagation of the wave response to high latitudes and ultimately to the Antarctic stratosphere (i.e., the weak polar stratospheric temperature response indicated by the white square in Figure 12b). A zonal PSA-2-like wavetrain does appear in the B simulations, similarly to that seen in the F simulations, but with a smaller amplitude.
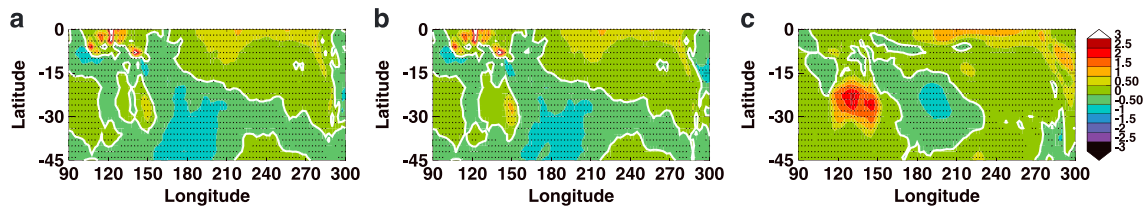

Figure 11. WPEN-NTRL 2 m temperature differences (K) in the equatorial and South Pacific in austral spring, for (a) P_W-P_N, (b) $IDEAL_W$-P_N, and (c) F_W-F_N. Black crosses indicate differences significant at the 95% level, in a two-tailed t test. White contours denote zero difference.

Table 4. SST Anomalies in the Niño 4 and Niño 3.4 Region

Pairs of Simulations	SON		DJF	
	Niño–4	Niño–3.4	Niño–4	Niño–3.4
P, FCLI, A	0.76	0.97	0.89	1.60
$IDEAL_W\text{-}P_N$	0.73	0.96	0.83	1.54
F, FSST	0.76	0.90	0.83	0.90
B	0.96	0.89	0.73	0.57
C	0.73	0.92	0.69	0.61

4. Summary and Discussion

[38] The late 21st century atmospheric response to warm pool El Niño events was investigated with a set of GEOSCCM simulations. Pairs of 50 year time slice provided large samples of the response to ENSO neutral and WPEN conditions, in both present-day and in projected late 21st century climate conditions. The GEOSCCM can simulate the observed, present-day response to WPEN events when forced by observed SST fields [*Hurwitz et al.*, 2011b; *Garfinkel et al.*, 2012]. For the GEOSCCM simulations of the future, late 21st century sea surface temperatures and sea ice concentrations, an existing ocean-atmosphere simulation were prescribed as boundary conditions (Figure 2), in addition to projected 2100 concentrations of the primary greenhouse gases and ozone-depleting substances. Despite known ocean-atmosphere model biases, the prescribed SST fields represent a best estimate of the structure of late 21st century WPEN events. In the Arctic, the polar vortex weakened in response to WPEN events, as for conventional El Niño events [*Herceg Bulic et al.*, 2012], though the late winter response to WPEN events was not as strong as that in a contemporary climate. The Antarctic vortex weakened in response to WPEN events in the present-day climate but did not weaken or warm in response to WPEN events in a future climate (Figures 3 and 4).

[39] The combined impact of increasing GHGs and decreasing ODSs on the polar stratosphere on the response to WPEN was negligible, despite large differences between the present-day and projected future climates (Figure 1). That is, when present-day SSTs were prescribed, the polar response to WPEN (both in the Arctic and Antarctic) was the same in both present-day and future climate conditions: strong planetary wave driving and weakening of both polar vortices during the extended boreal winter season (e.g., Tables 2 and 3).

[40] The Arctic stratospheric responses to WPEN were qualitatively similar under present-day and future climate conditions. The weaker magnitude of the late winter Arctic response reflected the relatively weaker midwinter forcing by SSTs in the Niño 3.4 region in the modeled late 21st century SSTs as compared with the present-day SSTs (Figures 2 and 12a). Results of an idealized WPEN simulation suggested that SSTs outside of the tropical Pacific have a minor influence on the magnitude of the Arctic stratospheric response.

[41] The nonresponse of the Antarctic stratosphere to WPEN events, in a future climate, reflected simulated future changes in the tropospheric teleconnections. The present-day SH response to WPEN was characterized by a strong, poleward (PSA-1-like) wavetrain in the upper troposphere and an enhancement of tropospheric eddy heat flux entering the

polar stratosphere. In the future climate simulations, the poleward wave response weakened and a zonal wave response (PSA-2-like) appeared in austral spring (Figures 4 and 8). In this modeling framework, it was not possible to completely separate the impacts of future SSTs from those of future climate conditions, since the climate conditions feedback to the ocean surface and influence the resulting SST fields. Nevertheless, sensitivity simulations, in which the prescribed SSTs and radiatively active gases were varied in separate simulations, provided insight into the qualitative impacts of the modeled SST fields and climate forcings. These simulations revealed that the simulated future South Pacific SSTs, rather than the increases in GHGs and decreases in ODSs, caused the change in WPEN teleconnection pattern (Figure 12b). Weakening of the poleward wavetrain was consistent with a marked weakening of the convective response to WPEN in the southeastern South Pacific Convergence Zone (Figure 10). Similar changes in the upper tropospheric teleconnections were found in simulations forced by a different set of modeled 21st century SSTs. In isolation, Antarctic ozone recovery had a negligible impact on the polar stratospheric response to WPEN.

[42] The appearance of the PSA-2-like pattern and positive geopotential height response at 30°S, 120°E, when future SSTs were prescribed, reflected strong heating over the Australian continent (Figures 5 and 11). While it is beyond the scope of this paper to determine the cause of this Australian heating or how likely such a heating response to
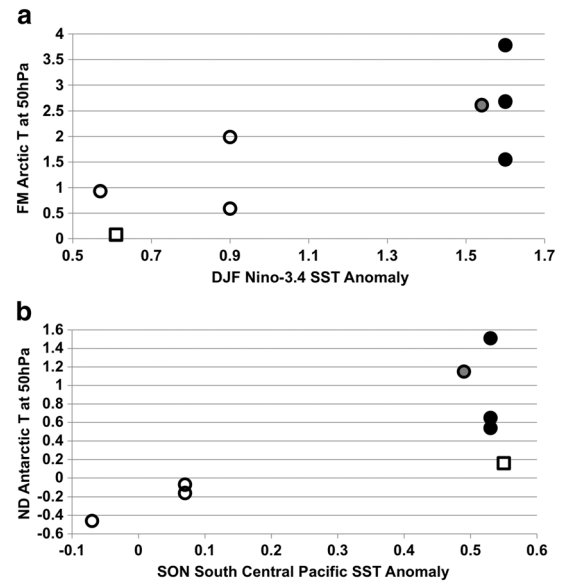
Figure 12. Scatter plots showing the relationship between (a) DJF seasonal mean SST anomaly in the Niño 3.4 region and the February/March Arctic polar cap temperature response at 50 hPa and (b) the SON seasonal mean SST anomaly in the south central Pacific (180–220°E, 5–15°S) and the November/December Antarctic polar cap temperature response at 50 hPa. Each symbol represents the mean difference between WPEN and NTRL simulations: Black circles indicate simulations forced by observed SSTs (P, FCLI, and A). Grey circles indicate $IDEAL_W\text{-}P_N$ differences. White circles indicate the simulations forced by CCSM3 SST fields (FSST, F, and C). White squares indicate $B_W\text{-}B_N$ differences.

WPEN is to occur in a future climate, *Watterson* [2012] found that future Australian warm climate regimes are related to relatively warmer SSTs in the central and western equatorial Pacific and eastern Indian oceans. Furthermore, the PSA-2 pattern is strongly correlated with SSTs in the Indian Ocean and surrounding Australia [*Mo and Paegle*, 2001].

[43] The above results motivate further study with a coupled ocean-atmosphere CCM. Planned simulations with a new ocean-atmosphere formulation of the GEOSCCM will investigate the Australian climate response to changes in nearby SSTs, considering atmosphere-land-ocean feedbacks, as well as the stratospheric response to various types of ENSO events that are generated interactively by the model. SST biases, particularly in the Niño 3.4 and south-central Pacific regions, will need to be considered in interpreting the modeled atmospheric response to ENSO.

References

Arblaster, J. M., G. A. Meehl, and D. J. Karoly (2011), Future climate change in the Southern Hemisphere: Competing effects of ozone and greenhouse gases, *Geophys. Res. Lett.*, 38, L02701, doi:10.1029/2010GL045384.

Ashok, K., S. K. Behera, S. A. Rao, H. Weng, and T. Yamagata (2007), El Niño Modoki and its possible teleconnections, *J. Geophys. Res.*, 112, C11007, doi:10.1029/2006JC003798.

Collins, M. (2000), The El Niño–Southern Oscillation in the second Hadley Centre coupled model and its response to greenhouse warming, *J. Clim.*, 13, 1299–1312, doi:10.1175/1520–0442(2000)013<1299:TENSOO>2.0.CO;2.

Garfinkel, C. I., M. M. Hurwitz, D. W. Waugh, and A. H. Butler (2012), Are the teleconnections of central pacific and eastern pacific El Niño distinct in boreal wintertime?, *Clim. Dyn.*, 1–18, doi:10.1007/s00382-012-1570-2.

Graf, H.-F., and D. Zanchettin (2012), Central Pacific El Niño, the subtropical bridge, and Eurasian climate, *J. Geophys. Res.*, 117, D01102, doi:10.1029/2011JD016493.

Hegyi, B., and Y. Deng (2011), A dynamical fingerprint of tropical Pacific sea surface temperatures in the decadal-scale variability of the cool-season Arctic precipitation, *J. Geophys. Res.*, 116, D20121, doi:10.1029/2011JD016001.

Herceg Bulic, I., C. Brankovic, and F. Kucharski (2012), Winter ENSO teleconnections in a warmer climate, *Clim. Dyn.*, 38, 1583–1613, doi:10.1007/s00382-010-0987-8.

Hitchcock, P., T. G. Shepherd, and C. McLandress (2009), Past and future conditions for polar stratospheric cloud formation simulated by the Canadian Middle Atmosphere Model, *Atmos. Chem. Phys.*, 9, 483–495.

Hurwitz, M. M., and P. A. Newman (2010), 21st century trends in Antarctic temperature and polar stratospheric cloud (PSC) area in the GEOS chemistry-climate model, *J. Geophys. Res.*, 115, D19109, doi:10.1029/2009JD013397.

Hurwitz, M. M., P. A. Newman, L. D. Oman, and A. M. Molod (2011a), Response of the Antarctic stratosphere to two types of El Niño events, *J. Atmos. Sci.*, 68, 812–822, doi:10.1175/2011JAS3606.1.

Hurwitz, M. M., I.-S. Song, L. D. Oman, P. A. Newman, A. M. Molod, S. M. Frith, and J. E. Nielsen (2011b), Response of the Antarctic stratosphere to warm pool El Niño events in the GEOS CCM, *Atmos. Chem. Phys.*, 11, 9659–9669, doi:10.5194/acp-11-9659-2011.

Hurwitz, M. M., P. A. Newman, and C. I. Garfinkel (2012), On the influence of North Pacific sea surface temperatures on the arctic winter climate, *J. Geophys. Res.*, 117, D19110, doi:10.1029/2012JD017819.

Hurwitz, M. M., L. D. Oman, P. A. Newman, and I.-S. Song (2013), Net influence of an internally–generated QBO on stratospheric climate and chemistry, *Atm. Phys. Chem.*, 13, 12,187–12,197, doi:10.5194/acp-13-12187-2013.

Jin, F.-F., and B. J. Hoskins (1995), The direct response to tropical heating in a baroclinic atmosphere, *J. Atmos. Sci.*, 52, 307–319.

Johns, T. C. (2006), The new Hadley Centre climate model HadGEM1: Evaluation of coupled simulations, *J. Clim.*, 19(7), 1327–1353.

Kawa, S. R., R. Bevilacqua, J. J. Margitan, A. R. Douglass, M. R. Schoeberl, K. Hoppell, and B. Sen (2003), The interaction between dynamics and chemistry of ozone in the set–up phase of the Northern Hemisphere polar vortex, *J. Geophys. Res.*, 108(D5), 8310, doi:10.1029/2001JD001527.

Kiehl, J. T., C. A. Shields, J. A. Hack, and W. D. Collins (2006), The climate sensitivity of the Community Climate System Model version 3 (CCSM3), *J. Clim.*, 19, 2584–2596.

Kug, J.-S., F.-F. Jin, and S.-I. An (2009), Two types of El Niño events: Cold tongue El Niño and warm pool El Niño, *J. Clim.*, 22, 1499–1515.

Kug, J.-S., S.-I. An, Y.-G. Ham, and I.-S. Kang (2010), Changes in El Niño and La Niña teleconnections over Pacific-North America in the global warming simulations, *Theor. Appl. Climatol.*, 100, 275–282, doi:10.1007/s00704-009-0183-0.

Larkin, N. K., and D. E. Harrison (2005), On the definition of El Niño and associated seasonal average U.S. weather anomalies, *Geophys. Res. Lett.*, 32, L13705, doi:10.1029/2005GL022738.

Mo, K. C. (2000), Relationships between low-frequency variability in the Southern Hemisphere and sea surface temperature anomalies, *J. Clim.*, 13, 3599–3610.

Mo, K. C., and J. N. Paegle (2001), The Pacific-South American modes and their downstream effects, *Int. J. Climatol.*, 21, 1211–1229, doi:10.1002/joc.685.

Molod, A., L. Takacs, M. Suarez, J. Bacmeister, I.–S. Song, and A. Eichmann (2012), The GEOS-5 Atmospheric General Circulation Model: Mean Climate and Development from MERRA to Fortuna, Tech. Rep. Series on Global Modeling and Data Assimilation, Vol. 28.

Müller, W. A., and E. Roeckner (2006), ENSO impact on midlatitude circulation patterns in future climate change projections, *Geophys. Res. Lett.*, 33, L05711, doi:10.1029/2005GL025032.

Newman, P. A., E. R. Nash, and J. E. Rosenfield (2001), What controls the temperature of the Arctic stratosphere during the spring?, *J. Geophys. Res.*, 106, 19,999–20,010, doi:10.1029/2000JD000061.

Pawson, S., R. S. Stolarski, A. R. Douglass, P. A. Newman, J. E. Nielsen, S. M. Frith, and M. L. Gupta (2008), Goddard Earth Observing System chemistry-climate model simulations of stratospheric ozone-temperature coupling between 1950 and 2005, *J. Geophys. Res.*, 113, D12103, doi:10.1029/2007JD009511.

Polvani, L. M., M. Previdi, and C. Deser (2011), Large cancellation, due to ozone recovery, of future Southern Hemisphere atmospheric circulation trends, *Geophys. Res. Lett.*, 38, L04707, doi:10.1029/2011GL046712.

Rasmusson, E. M., and T. H. Carpenter (1982), Variation in tropical sea surface temperature and surface wind fields associated with Southern Oscillation/El Niño, *Mon. Weather Rev.*, 110, 354–384.

Rayner, N. A., D. E. Parker, E. B. Horton, C. K. Folland, L. V. Alexander, D. P. Rowell, E. C. Kent, and A. Kaplan (2003), Global analyses of sea surface temperature, sea ice, and night marine air temperature since the late nineteenth century, *J. Geophys. Res.*, 108, 4407, doi:10.1029/2002JD002670.

Rienecker, M. M., et al. (2008), The GEOS–5 Data Assimilation System—Documentation of versions 5.0.1, 5.1.0, and 5.2.0, NASA Technical Report Series on Global Modeling and Data Assimilation, V27.

Schneider, D. P., Y. Okumura, and C. Deser (2012), Observed Antarctic interannual climate variability and tropical linkages, *J. Clim.*, 25, 4048–4066, doi:10.1175/JCLI-D-11-00273.1.

Solomon, S., D. Qin, M. Manning, Z. Chen, M. Marquis, K. B. Averyt, M. Tignor, and H. L. Miller (Eds) (2007), *Contribution of Working Group I to the Fourth Assessment Report of the Intergovernmental Panel on Climate Change (IPCC)*, Cambridge Univ. Press, Cambridge, United Kingdom and New York, N.Y., U.S.A.

Song, H.-J., E. Choi, G.-H. Lim, Y. H. Kim, J.-S. Kug, and S.-W. Yeh (2011), The central Pacific as the export region of the El Niño–Southern Oscillation sea surface temperature anomaly to Antarctic sea ice, *J. Geophys. Res.*, 116, D21112, doi:10.1029/2011JD015645.

Stratospheric Processes and their Role in Climate (SPARC) Chemistry–Climate Model Validation (CCMVal) (2010), SPARC report on the evaluation of chemistry–climate models, Ed. V. Eyring, T. G. Shepherd, and D. W. Waugh, SPARC Rep. No. 5, WCRP–132, WMO/TD–No. 1526.

Stevenson, S. L. (2012), Significant changes to ENSO strength and impacts in the twenty-first century: Results from CMIP5, *Geophys. Res. Lett.*, 39, L17703, doi:10.1029/2012GL052759.

Vera, C., G. Silvestri, V. Barros, and A. Carríl (2004), Differences in El Niño response over the Southern Hemisphere, *J. Clim.*, 17, 1741–1753.

Watterson, I. G. (2012), Understanding and partitioning future climates for Australian regions from CMIP3 using ocean warming indices, *Clim. Change*, 111, 903–922.

World Meteorological Organization (WMO) (2011), Scientific assessment of ozone depletion: 2010, Global Ozone Research and Monitoring Project, Rep. No. 52, 516 pp., Geneva.

Xie, F., J. Li, W. Tian, J. Feng, and Y. Han (2012), Signals of El Niño Modoki in the tropical tropopause layer and stratosphere, *Atmos. Chem. Phys.*, 12, 5259–5273, doi:10.5194/acp-12-5259-2012.

Xie, S.-P., C. Deser, G. A. Vecchi, J. Ma, H. Teng, and A. T. Wittenberg (2010), Global warming pattern formation: Sea surface temperature and rainfall, *J. Clim.*, 23(4), 966–986, doi:10.1175/2009JCLI3329.1.

Yeh, S.-W., B. Y. Yim, Y. Noh, and B. Dewitte (2009), Changes in mixed layer depth under climate change projections in two CGCMs, *Clim. Dyn.*, 33, 199–213, doi:10.1007/s00382-009-0530-y.

Zubiaurre, I., and N. Calvo (2012), The El Niño–Southern Oscillation (ENSO) Modoki signal in the stratosphere, *J. Geophys. Res.*, 117, D04104, doi:10.1029/2011JD016690.